Malaysian Journal of Soil Science 2026 Vol. 30: 192-205
Received 1/3/2026; Revised 17/4/2026; Accepted 14/7/2026; Online 12/8/2026

Small-Scale Biochar Synthesis Using a Simple Rotary Kiln: Characteristics of Products Derived from Several Agricultural Wastes in the Semi-Arid Tropical Environment of Lombok, Indonesia

Sukartono[1]; Jaya, Dori Kusuma[2,3]*; Susilowati, Lolita Endang[2]; Azizah, Isnaniar Rahmatul[2]; Dewi, Intan Lusiana[2]; Kusumo, Bambang Hari[2]; & Yusiharni, Emielda[4]

[1]Centre for Sustainable Farm Systems (CESFARM), University of Mataram, Mataram, Indonesia
[2]Department of Soil Science, Faculty of Agriculture, University of Mataram, Mataram, Indonesia
[3]UWA School of Agriculture and Environment, The University of Western Australia, Perth, Australia
[4]UWA XRD Facility, Material & Environmental Analysis Platform, The University of Western Australia, Perth, WA, Australia

*Correspondence: dori_jaya@unram.ac.id

ABSTRACT

Open-field burning of agricultural residues remains a common practice in Indonesian farming systems and contributes to environmental degradation. Converting these biomasses into biochar using a simple instrument is likely to benefit smallholder farmers in semi-arid tropical regions. This study characterises biochar produced in Lombok Island from four locally abundant feedstocks (Rice Husk (RH), Corn Cob (CC), Coconut Fibre (CF), Tobacco Stem (TS)). Analysis by SEM, BET, FTIR, and XRD shows these biochars have different properties as a function of feedstock type and pyrolysis conditions. SEM revealed varying porous structures; CC had the widest pores. BET showed that TS biochar had the highest surface area (17.08 $m^2\ g^{-1}$) and the longest pyrolysis time (59 min), whereas CC had the lowest surface area (5.74 $m^2\ g^{-1}$) and the shortest pyrolysis time (14 min). FTIR analysis revealed that all biochars share key functional groups (-OH, C=C, C-H) but also exhibit feedstock-specific traits. RH and CC are rich in silica (Si-O-Si), CF contains complex oxygen groups, and TS has a stable aromatic structure. These findings suggest that RH biochar is suited for inorganic adsorption and as a silica soil amendment, CC for organic molecule adsorption, and CF/TS biochars for long-term soil carbon sinks and CEC enhancement. This work provides practical guidance for selecting biochar types for agricultural and environmental applications.

Keywords: BET, biochar, FTIR, local feedstocks, simple instrument

INTRODUCTION

The increasing production and poor management of agricultural wastes, such as open-field burning, remain a major environmental issue in many developing countries, particularly in Indonesia. This practice primarily contributes significantly to air pollution and greenhouse gas (GHG) emissions, leading to a rise in global surface temperatures that threatens ecosystem degradation (Permadi & Oanh, 2013; Reddy et al., 2025). Beyond these general environmental concerns, land degradation and declining soil quality represent other main problems associated with improper agricultural waste management (Meena et al., 2025). A direct observable impact on soil characteristics is the reduction of soil carbon stocks due to burning practices, lower input of soil organic matter, and a decrease in soil pH resulting from the continuous and imbalanced application of inorganic fertilisers. These factors can ultimately disrupt the growth and production of crops cultivated on such degraded land (Zhang et al., 2022).

Several types of feedstocks derived from agricultural residues, including rice husk, corn cobs, coconut fibre, and tobacco stems, are abundant in Indonesia, particularly in West Nusa Tenggara (WNT) province. Fitri et al. (2023) reported that the production of these waste materials in WNT reaches approximately 16%, 88.25%, 64.91%, and 85%, respectively. This abundance of agricultural residues presents a significant opportunity to process them into valuable products, such as biochar, for various applications, including use as soil amendments. Biochar synthesis through pyrolysis is increasingly promoted as a sustainable alternative to open burning. It offers both soil quality improvement and carbon sequestration. Many studies confirm that biochar application can enhance soil health and quality, promote microbial activity, and improve crop productivity (Kabir et al., 2023; Kerner et al., 2023; Ighalo et al., 2025). Biochar is a carbon-rich by-product of pyrolysis, a process that heats organic biomass under low-oxygen conditions. It gained significant scientific interest after studies of the highly fertile "Terra Preta" soils in the Amazon Basin (Glaser *e*t al., 2001). Its stable carbon structure allows it to act as an effective long-term carbon sink (Baldock & Smernik, 2002). It also provides ecological benefits, such as reducing methane emissions and promoting sustainable agricultural practices (Sriphirom et al., 2022). Biochar has a highly stable structure and resists microbial decomposition for decades. However, its stability depends on the pyrolysis parameters, including temperature, feedstock type, and residence time (Jia et al., 2018; Almutairi et al., 2023). Three key compositional factors in the feedstock–cellulose, hemicellulose, and lignin–influence biochar stability. The nature of the feedstock is especially important (Tag et al., 2016). Using abundant local waste materials provides a viable option for producing biochar with favourable structure, surface area, functional groups, elemental co-location, and proximate composition.

Despite these well-documented advantages, many smallholder farmers in rural areas of Indonesia still rely on open burning to manage crop residue rather than processing it into biochar as a soil amendment. In addition, adoption of biochar among smallholder farmers remains limited due to the technical complexity and high operational costs of modern pyrolysis technologies. Consequently, simple techniques have recently attracted growing attention among local communities. However, relatively few studies have evaluated low-technology biochar production methods, particularly the biochar produced by these methods for soil and environmental applications in tropical areas. Therefore, the objective of this study is to characterise the biochar produced from four different feedstocks using a simple rotary kiln and to discuss potential benefits for soil amendment or carbon sequestration.

MATERIALS AND METHODS

Collection of Agricultural Feedstocks and Preparation

The feedstocks for biochar production are obtained from four local agricultural wastes abundant in the farmlands of Lombok Island, West Nusa Tenggara province: Rice Husk (RH), Corn Cob (CC), Coconut Fibre (CF), and Tobacco Stem (TS). These crop biomasses are derived from post-harvested agricultural residues. A total of 25 kg of each raw material was collected from major agricultural areas across Lombok Island. The materials were air-dried for several days and cleaned mechanically to remove any remaining dirt. The dried feedstocks were then cut into smaller pieces, approximately 5-10 cm in length, to improve heat exposure during pyrolysis. Afterwards, the dried samples underwent biochar pyrolysis.

Biochar Synthesis

Biochar was produced using a simple rotary-kiln pyrolysis system designed by the Soil Physics Laboratory at the Faculty of Agriculture, University of Mataram (Figure 1). The chopped agricultural residues were loaded into a metal reactor drum, which was then heated externally using firewood under oxygen-limited conditions. The temperature inside the reactor was gradually increased to reach 210-300°C. The pyrolysis process continued until the target temperature was reached, and the biochar formation indicator was observed, including thick smoke emission and the conversion of the feedstocks into black char, which indicated biochar maturity. After production, the product was sprayed with water to prevent further ash formation, cooled, and air-dried. After that, the biochar was weighed, ground, sieved, and analysed downstream. The biochars were then termed as Rice Husk Biochar (RHB), Corn Cob Biochar (CCB), Coconut Fibre Biochar (CFB), and Tobacco Stem Biochar (TSB).

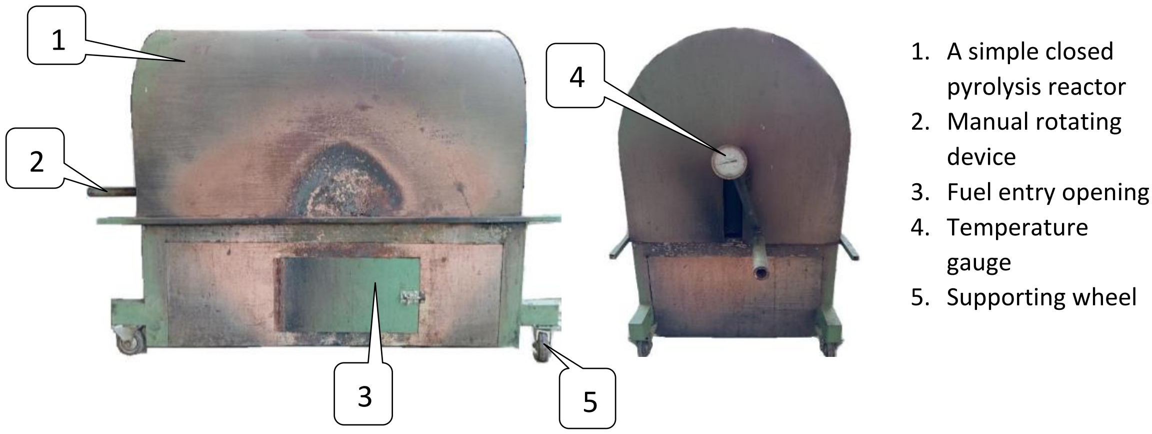

Figure 1. Simple rotary kiln for producing biochar

Proximate and Chemical Analysis
Laboratory analyses of each biochar sample, including moisture, ash content, volatile matter, fixed carbon, pH, Electrical Conductivity (EC), and Cation Exchange Capacity (CEC), were conducted. Proximate estimation was measured using the ASTM D1762-84 procedure, while fixed carbon was calculated by the difference according to proximate content as follows: fixed carbon (%) = 100 – (moisture (%) + volatile matter (%) + ash (%)). The pH of biochar was measured in a 1:5 (w/v) suspension in distilled water and in a 1:5 (w/v) suspension in KCl solution, while the EC was measured in a 1:5 (w/v) suspension in distilled water. Whereas CEC was determined using the ammonium acetate (NH_4OAc) saturation method at pH 7.

Biochar Characterisation
Biochar characterisation was conducted through several methods. The surface morphology and structure of the biochar material were observed using a Scanning Electron Microscope (SEM) with a JEOL JCM-7000 instrument. Surface area and pore size were analysed using the Brunauer-Emmett-Teller (BET) equation and were evaluated by the t-plot method. Qualitative analysis of the functional groups or chemical bonds present in each biochar was performed using Fourier Transform Infrared (FTIR) analysis with a Shimadzu Model 5020 FTIR Spectrometer (absorbance spectra wave number 400 to 4,000 cm^{-1}), and the spectral data were further processed using Omnic 9.0 (Thermo Scientific Nicolet iS10). For the crystalline structure, XRD (X-ray diffraction) analysis of the biochar powder was conducted using a Bruker AXS D8 Advance Eco with 25 mA Cu Kα radiation at a scan speed of 2 degrees min-1 in continuous-scan mode to analyse the mineralogy of the samples.

RESULTS AND DISCUSSION

Proximate and Chemical Analysis
Table 1 presents the results of proximate and chemical analyses of four biochar samples produced under different pyrolytic conditions, focusing on moisture, ash content, volatile matter, fixed carbon, pH, EC, and CEC. With respect to heating temperature, biochars produced at higher temperature (300 °C) showed significantly lower moisture, ash content, and volatile

matter compared to those synthesised at 210°C. This results in the lowest proportion of fixed carbon in the RHB samples.

In detail, RHB produced at 210 °C performed the highest percentage of moisture (26.48%), ash content (40.60%), and volatile matter (66.81%) among all samples, compared to those produced at a higher temperature (300°C). These results indicate limited thermal decomposition in RHB. By comparison, the other three samples, namely CCB, CFB, and TSB, demonstrated significantly improved proximate properties. CCB recorded the lowest moisture content of 6.92% and a minimal ash content of 7.43%, while having a high volatile matter content of 37.23%. These results are consistent with CFB, which exhibits slightly higher water content (9.19%) but higher volatile compound content (48.87%) at a residence time of 19 minutes. In contrast, a longer pyrolytic time of 59 minutes in TSB leads to notable increases in water and ash content of 25.93% and 23.19%, respectively, while volatile matter decreases to 34.13%. This result suggests that the labile carbon fraction remains incompletely degraded even during extended heating. To conclude, thermal exposure has a stronger effect on the proximate composition than pyrolytic time. This result corresponds to the findings by Kim et al., 2012, Zhao et al., 2018, and Raza et al., 2021.

Table 1. Proximate and chemical analysis of the produced biochars at different pyrolytic conditions

Parameter	Samples			
	RHB	**CCB**	**CFB**	**TSB**
Temperature (°C)	210	300	300	300
Residence time (min)	43	14	19	59
Water content (%)	26.48	6.92	9.19	25.93
Ash content (%)	40.60	7.43	4.71	23.19
Volatile matter (%)	66.81	37.23	48.87	34.13
Fixed carbon (%)	ND*	48.42	37.22	16.75
pH H_2O	7.26	8.16	8.88	9.42
pH KCl	6.23	7.64	8.12	9.25
ΔpH	1.03	0.52	0.76	0.18
EC (dS/m)	0.289	0.605	0.027	0.097
CEC (meq/100 g)	45.54	27.92	55.13	89.08

*ND: Not determined

The chemical properties (i.e, pH, CEC, and EC) of the biochars are also presented in **Table 1**. In general, higher pyrolysis temperatures and longer processing times resulted in more alkaline biochars with lower ΔpH values and a remarkably enhanced CEC. Meanwhile, EC values varied among biochar samples and did not show a linear trend with processing time. Specifically, RHB exhibits the lowest alkalinity with pH H_2O of 7.26 and pH KCl of 6.23, alongside the widest ΔpH of 1.03. This relatively large value indicates a majority of negatively charged sites, such as silica-containing ions and oxygen (Kome et al., 2018). The RHB sample also recorded a moderate EC and CEC value of 0.289 $dS.m^{-1}$ and 45.54 meq/100 g, respectively. By contrast, the biochar produced at 300°C for 14 minutes exhibits progressively higher pH. CCB has a pH H_2O value of 8.16, a reduced ΔpH of 0.52, and an EC of 0.0605 $dS.m^{-1}$, while showing the lowest CEC of 27.92 meq/100 g. Compared to CCB, the generated CFB for 19 minutes demonstrates a further rise in pH H_2O to 8.88 and a lower ΔpH (0.76), followed by a notably reduced EC of 0.027 $dS.m^{-1}$ and a higher CEC value (55.13 meq/100 g). The longest pyrolytic time observed in TSB, 59 minutes, yields the most alkaline biochar, with a pH of 9.42 in water, the lowest ΔpH (0.18), and the highest CEC of 89.08 meq/100 g. This indicates the development of functional groups and increased surface oxidation in extended thermal exposure. Therefore, pyrolytic conditions firmly affect the alkalinity and CEC of the biochar, which promotes more chemically reactive materials (Tomczyk et al., 2020; Prasiefa & Firmansyah, 2025).

Morphology of Biochar

Figure 2 demonstrates the microscopic morphology of the four different types of biochar (rice husk, corn cob, coconut fibre, and tobacco stem). The observed field of view reveals the interior structure of the biochar. Fundamentally, it exhibits a porous structure with varying sizes and patterns, revealing the special characteristics of each material. The pore structure transformations of all biochar samples were observed as a compacted structure in SEM images, indicating that temperatures of 210-300°C were not sufficiently high for pore development.

In depth, corn cob has the widest micropores at 26.67 µm, followed by coconut fibre (25.33 µm), tobacco stem (25 µm), and rice husk (18 µm). The micrograph of the corn cob presents largely fine cylindrical units on the surface (Gotore et al., 2022), while the others have a relatively thick wall, which may correspond to a high lignin and cellulose content. In **Figure 2a**, the RHB exhibits the most irregular and predominantly compact pore structure. It is characterised by tiny and discontinuous pores with sizes mostly below 10 µm. The pore walls appear thick and uneven, indicating limited devolatilization due to incomplete thermal degradation of organic constituents. This is typically associated with low temperature during the pyrolysis process, leading to insufficient pore development (Claoston et al., 2014). Thus, this biochar possesses a lower surface area and limited pore expansion, which may be effective for developed microbial colonisation in such micropores (Bu et al., 2019). In comparison, CCB in Figure 2b presents the appearance of a larger and more developed macropore structure, with pore sizes reaching about 14-27 µm. The walls of the pore become more well-defined, suggesting enhanced volatile matter emission. This indicates that higher temperature promotes pore structure reorganisation and expansion (Ahmad et al., 2012; Budai et al., 2016; Chatterjee et al., 2020). This condition is particularly beneficial for soil to have better aeration and water infiltration (Ghorbani et al., 2022). Developed pore evolution can also be seen in CFB (**Figure 2c**), where the biochar illustrates integrated pore networks and is well-structured with relatively uniform pore diameters (20-25 µm). The smoother interior pore surfaces indicate complete degradation of labile organic matter, as evidenced by the highest volatile matter proportion among all biochar samples (**Table 1**). It is important to note that TSB in Figure 2d provides a substantially thick pore boundary, which can be observed from the cross-section of the tobacco stem. This condition reflects the resistance of the biochar type during the extended pyrolytic process (Qin et al., 2016). It also has large pores ranging from 19-26 µm. The high stability of the pore may facilitate better pathways for water and gases to flow and play a key role in carbon sequestration (Kabir et al., 2023). In terms of soil amelioration, biochars exhibiting moderately large pores, as observed in **Figures 2b** and **2c**, are likely to facilitate an optimal balance between aeration, water retention, and microbial habitat, whereas densely structured biochars may offer limited functionality to some extent (Chen et al., 2024).

Surface Area and Pore Distribution

Brunauer-Emmett-Teller (BET) surface area of different types of biochar varied fundamentally depending on both the feedstock's intrinsic properties and the pyrolytic conditions (**Table 2**). This study found that the surface area of TSB increased the most (17.08 m^2 g^{-1}) when the pyrolysis time was extended to 59 minutes, while CCB exhibited the lowest value (5.74 m^2 g^{-1}) after 14 minutes of pyrolysis. The relatively longer retention time preferred surface area expansion and pore development (Irewale et al., 2025). However, the highest pore size of CCB and CFB is more affected by feedstock composition than by residence time (Kusnarta et al., 2024). These findings highlight that both pyrolysis parameters and the inherent feedstock properties of the biochar synergistically control surface area and pore development under the same heating condition, with vital implications for the application of biochar as a soil amendment, nutrient carrier, and/or biocarrier.

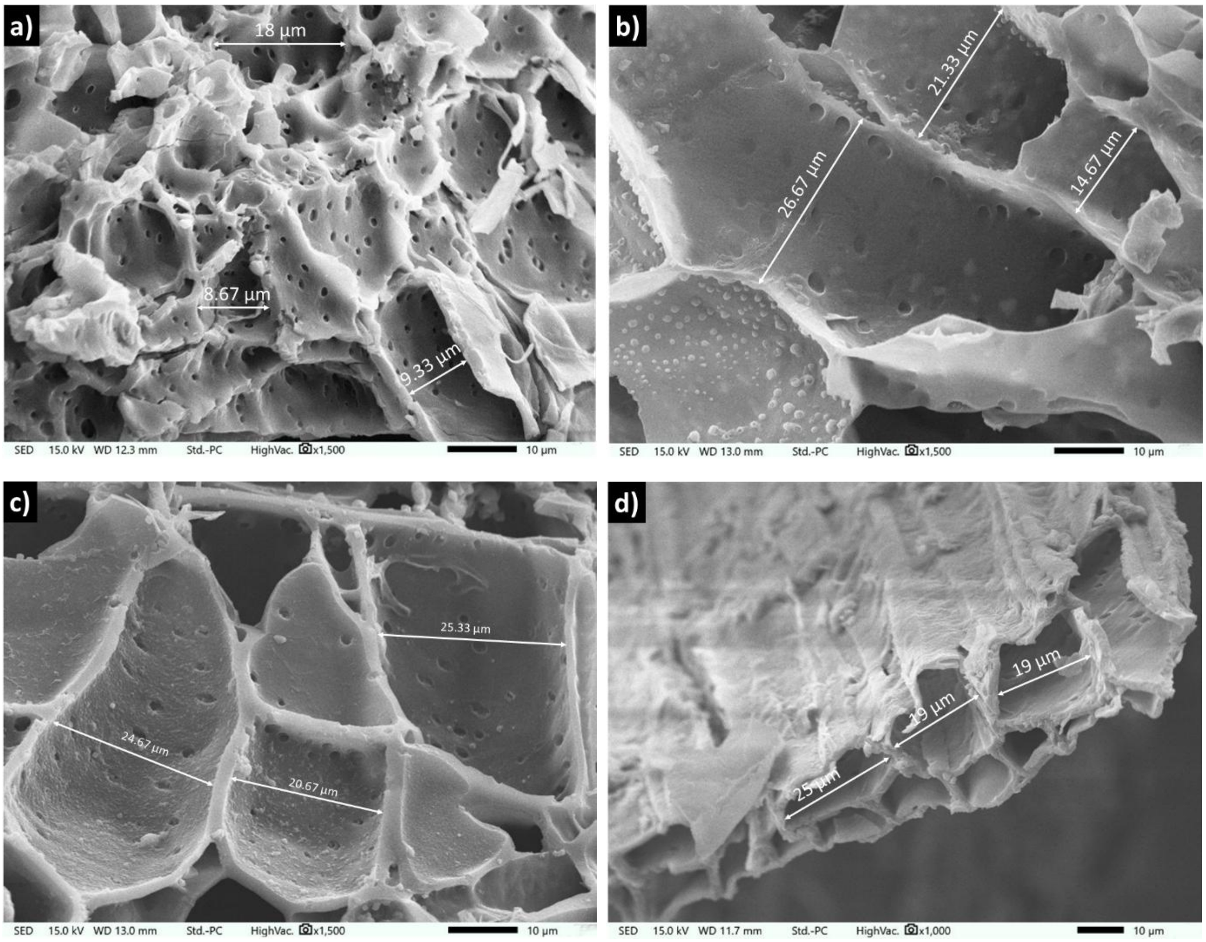

Figure 2. SEM images of four types of biochar. a) Rice Husk Biochar (RHB), b) Corb Cob Biochar (CCB), c) Coconut Fibre Biochar (CFB), d) Tobacco Stem Biochar (TSB)

Based on **Table 2**, the surface area and pore properties of the biochars clearly demonstrate the combination of pyrolytic residence time and temperature. The RHB exhibits a relatively low surface area of 13.06 m^2 g^{-1}, which can be attributed to the resistance of inherent plant-derived structures and to poor pore collapse under mild burning conditions (210°C). Consequently, this contributes to the lower average pore diameter and total micropore size (Yang et al., 2021; Handiso et al., 2024). In comparison, CCB produced at 300°C for a shorter time exhibits the lowest BET surface area of 5.74 m^2 g^{-1}. This condition indicates that insufficient pyrolytic time may inhibit pore opening despite the largest average pore size, resulting in incomplete connectivity and lower total micropore volume among the biochars. A similar trend was observed by Zhylina et al. (2025), who argued that the increase of BET surface area and pore volume with extended time reflects partial pore development under shorter residence times.

Table 2. BET surface area, pore volume, and diameter of the biochars under different pyrolytic conditions

Types of biochar	Temperature (°C)	Pyrolitic time (minutes)	BET area ($m^2.g^{-1}$)	Average pore size (Å)	Total micropore volume ($cm^3.g^{-1}$)
RHB	210	43	13.057	32.5752	0.01063
CCB	300	14	5.742	86.5008	0.01242
CFB	300	19	16.163	49.8764	0.02015
TSB	300	59	17.085	38.7078	0.01653

In particular, CFB and TSB produced with longer pyrolytic times for 19 and 59 minutes, respectively, show a substantial increase in BET surface areas (16.16-17.08 m^2 g^{-1}) along with larger average pore sizes and enhanced total micropore volumes. This trend illustrates that prolonged thermal exposure at moderate temperature induces progressive devolatilization and the formation of a pore network (Zhylina et al., 2025; Flores-izquierdo et al., 2025). Therefore, the results conclude that both residence time and temperature play a key role in regulating pore architecture and BET surface area. This highlights that the optimised residence time is also essential to improve physicochemical characteristics of biochar for multifunctionality, such as soil amendment.

FTIR Analysis

The FTIR absorbance spectra of four types of biochar are shown in **Table 3** and **Figure 3**. The FTIR analysis primarily identified functional groups at the char surface. Using the IR database USCS, we identify that all produced biochars exhibit broad spectral peaks between 3416.52 and 3415.75 cm^{-1}, assigned to the hydroxyl group (-OH). Peaks observed between 2957.04 and 2920.98 cm^{-1} are associated with aliphatic C-H groups, such as methylene (CH_2) and methyl (CH_3). The range at 1609.88-1512.53 cm^{-1} is probably due to the vibration of the aromatic C=C, whereas the lower peaks at 1492.53-1316.07 cm^{-1} belong to C-H bending, related to cellulose and lignin compounds present in the biochars (Tu et al., 2022; Goularte et al., 2025). The distinct functional groups among the biochars can be seen on the right-hand side of the peaks, which range from 2000 cm^{-1} to 500 cm^{-1}. Furthermore, the different compositions of feedstocks result in varying intensities and absorption bands that reflect different carbonisation levels, mineral content, and residual organic compounds.

Table 3. Functional group comparison of four types of biochar

Absorption peak (cm^{-1})				Major functional groups	Reference spectra				
Rice Husk	Corn Cob	Coconut Fibre	Tobacco Stem		Rice straw [a]	Corn straw [a]	Rice husk [b]	Coconut cloth bio-oil [c]	Tobacco [d]
3415.86	3415.75	3416.52	3416	-OH, -OH	3400s		3356	3446	3300s
2924.98	2956.75	2958.76	2957.04						
	2923.12	2920.98	2926.26	C-H stretching, -CH			2919	2926	
			2869.65		2800s	2800s		2856	2300s
1694.80	1694.63			C=O stretching				1645	1700s
1609.88	1604.74			Aromatic C=C,	1600s		1623		1600s
1512.53	1512.54	1597.64	1589.82	C=O, C-C		1550s		1511	
1437.67	1492.58	1437.58	1408.19						
	1437.61	1377.67	1383.87	C-H bending, -CH	1350s	1350s	1523-1353		1300s
	1376.56		1316.07						
		1265.68	1273.69	C-O stretching				1270	
			1117.70					1105	1000s
1100.10	1100.06			Si-O-Si stretching, -			1054		
798.86	799.23			Si-O, -C-O-C-			793		
564.14	467.21			Si-O bending					
467.22									
		874.45	873.28						
		816.73	780.95	Aromatic C-H					
		755.59						756	
			618.68						
		588.64	573.18	Skeletal deformation					
		477.24	518.87						

Note: a) Tu et al., 2022; b) Goularte et al., 2025; c) Dai et al., 2020; d) Peng et al., 2025

In detail, the FTIR spectrum of RHB shows a strong absorption band at 3415.86 cm^{-1}, assigned to the -OH stretching vibration. Peak at 2924.98 cm^{-1} shows C-H aliphatic strain, while peak at 1609.88 cm^{-1} is related to C=C aromatic strain, which is derived from carbonised lignin. The most prominent peaks are located at 1100.10 cm^{-1} and 467.22 cm^{-1}, which correlate to Si-O-Si strain and Si-O flexure. This shows the dominance of silica (SiO_2), a characteristic of rice husk. The presence of -OH and C-H groups indicates that a small part of the organic compound still exists, although its intensity is relatively low. This indicates that the pyrolysis process has produced a high level of carbonised biochar and dominant silica content, resulting in high potential rice husk biochar as a heavy metal adsorbent and silicate soil amendment (Severo et al., 2020; Burachevskaya et al., 2023).

The FTIR spectra of CCB also show an absorbed band at 3415.75 cm^{-1} for hydroxyl (-OH), 2923.12 and 2856.75 cm^{-1} for aliphatic (C-H), and 1604.74 cm^{-1} for aromatic (C=C). The band at 1492.53 and 1376.56 cm^{-1} indicates C-H bending, while the bands at 1100.06 cm^{-1} and 799.23 cm^{-1} indicate the presence of the Si-O-Si functional group. Moreover, the peak at 467.21 cm^{-1} indicates aromatic wave or minor mineral (Najafi-ghiri et al., 2025). The existence of a strong absorbed band at 1600-1000 cm^{-1} illustrates that this biochar still contains lignocellulose, which is not fully carbonised. This indicates a medium carbonisation level with a relatively high oxygen functional group content. Therefore, this biochar has a high potential as an organic adsorbent for improving CEC in the soil (Ali et al., 2021; Yuniwati & Lestari, 2021).

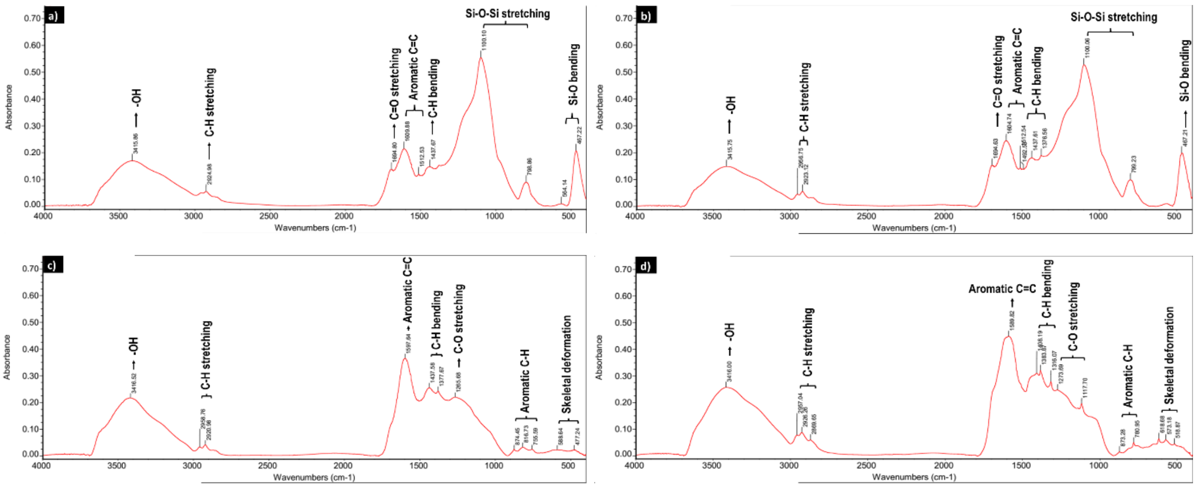

Figure 3. Absorbance with FTIR analysis of four types of biochar. a) RHB, b) CCB, c) CFB, d) TSB

Coconut Fibre Biochar (CFB) absorption pattern also performs common bands at 3416 cm^{-1} (-OH stretch), 2958.76 and 2920.98 cm^{-1} (C-H aliphatic), 1597.64 cm^{-1} (C=C aromatic), as well as 1437.58 and 1377.67 cm^{-1} (C-H bending). Additional band at 1265.68 cm^{-1} related to C-O stretching form ester or phenolic group, whereas the band between 816.73 and 755.59 cm^{-1} indicates the vibration of aromatic C-H (Sukartono et al., 2011; Zhang et al., 2018; Dai et al., 2020; Dhar et al., 2020). The number of -OH and C-O groups remaining indicates a fair carbonisation level, with high functional oxygen content. This condition makes CF biochar very promising to increase soil microbial activities, increase nutrient retention, and stimulate the development of soil aggregates (de Carvalho Junior et al., 2019; Guarnieri et al., 2021).

The FTIR spectrum of TSB visualises bands at 3416 cm^{-1} (-OH), 2957.04 and 2869.65 cm^{-1} (C-H aliphatic), and 1589.82 cm^{-1} (C=C aromatic). Beyond those bands, they are at 1408.19, and 1316.07 cm^{-1} indicates the presence of the C-H bending group, while bands 1273.69 cm^{-1}-1117.70 cm^{-1} are related to C-O stretching. Moreover, the band at 873.28-518.87 cm^{-1} illustrates C-H aromatic vibration. The abundance of oxygen-containing functional groups in CFB is higher than that in RHB and CCB. This pattern reflects that the TS biochar has a strong and stable aromatic structure, indicating a high level of carbonisation (Yıldız & Ceylan, 2018; Peng et al., 2025; Xu et al., 2025) and reactive domains. This characteristic creates biochar resistant to microbial decomposition, and it is very beneficial for soil carbon sequestration and long-lasting soil amendment (Ernest et al., 2024; Gross et al., 2024) as well as soil fertility improvement (Li et al., 2021; Zhao et al., 2021).

As described in the FTIR interpretation, rice husk biochar is characterised by the predominance of silicate. Corn cob exhibits a balance of mineral and organic groups, which indicates a moderate pyrolysis rate. Coconut fibre biochar provides the highest number of polar active molecules, reflecting its most chemically reactive properties. Meanwhile, tobacco stem biochar has sharp, stable, and diverse aromatic peaks, indicating high stability and polymerised carbon. Therefore, the fingerprint region from 1600 to 400 cm^{-1} is the main determinant for distinguishing the four types of biochar. Rice husk is mineralic, coconut fibre and corn cob are organically active, and tobacco stem is aromatically stable, each possessing distinct functional characteristics for agriculture and the environment.

XRD Analysis

The XRD patterns for RHB, CCB, CFB, and TSB are visualised in **Figure 4**. The broad main hump in the range 2θ = 10 ° to 30 ° corresponds to the (002) plane structure of the graphite carbon, reflecting the imperfect arrangement of carbon layers (amorphous carbon structure). This indicates that the formation of graphitic carbon of the lignocellulosic material during pyrolysis has not completely occurred (Mobarak *et al*., 2024). In addition, the four biochars have various degrees of crystallinity, showing RHB, CCB, DFB, and TSB the crystallinity values of 2,8%, 4,7%, 14,6, and 12,5%, respectively. This means that all biochar samples consist of most turbostratic carbon with a small percentage of crystalline domains. Furthermore, a weak secondary peak at approximately 2θ = 43-44° also seen in some samples, such as RHB and CCB, which corresponds to the (101 and 100) plane of disordered carbon. Thus, strengthening the existence of a partial crystalline phase (Vasilievici et al., 2025; Martín-Lara et al., 2026).

Of the four biochar samples, coconut fibre biochar demonstrates the highest crystallinity of 14.6%, which indicates the development of more ordered graphitic domains. This is likely because of the high content of the coconut fibre-derived lignin, which tends to facilitate aromatic condensation during the carbonisation process (Wood et al., 2024; Munzeiwa et al., 2025). Tobacco stem biochar also has a moderate crystallinity of 12.5%, indicating partial aromatisation under similar pyrolysis conditions. By contrast, rice husk biochar has the lowest crystallinity (2.8%), which can be attributed to its high silica content. This silica tends to create an amorphous SiO_2-C that limits the formation of regular carbon sheets (Hamidu et al., 2025; Kabore et al., 2026). Corn cob biochar also has low crystallinity (4.7%), reflecting that it contains rich cellulose, which can produce an amorphous carbon with more ease (Tomczyk et al., 2020).

Variations in crystallinity among biochars are influenced by the composition of agricultural biomass during the formation of carbon structures. The promotion of more ordered aromatic formation and graphitic structures is caused by the high lignin content, whereas high silica and ash composition tends to alter crystalline development. These structural variations have significant effects on the physicochemical characteristics of biochar, including its surface reactivity, CEC, and stability in soil environments (Khan et al., 2024; Nicholas et al., 2025; Anyebe et al., 2025). In rice husk and corn cob biochar, more amorphous components commonly have more active oxygenating sites and functional groups. Although amorphous structures are often associated with more oxygen-carrying functional groups, CEC is more strongly influenced by the accessibility and stability of these functional groups than by structural disorder alone (Tomczyk et al., 2020; Lago et al., 2021; Adhikari et al., 2024). In this study, biochars from coconut fibre and tobacco stems exhibit higher CEC and correspond to higher levels of aromatic C=C, -OH, and C-O functional groups in the FTIR analysis (Figure

3), despite their relatively higher crystallinity. This interpretation indicates that both biochars have persistent oxygen functional groups anchored within a stable aromatic carbon structure. Thus, they play a dominant role in improving soil fertility, such as CEC, despite their very high potential for long-term carbon sequestration in soil. These findings are consistent with the common properties of the lignocellulosic biomass-derived biochar at moderate pyrolysis temperature (Khan et al., 2024).

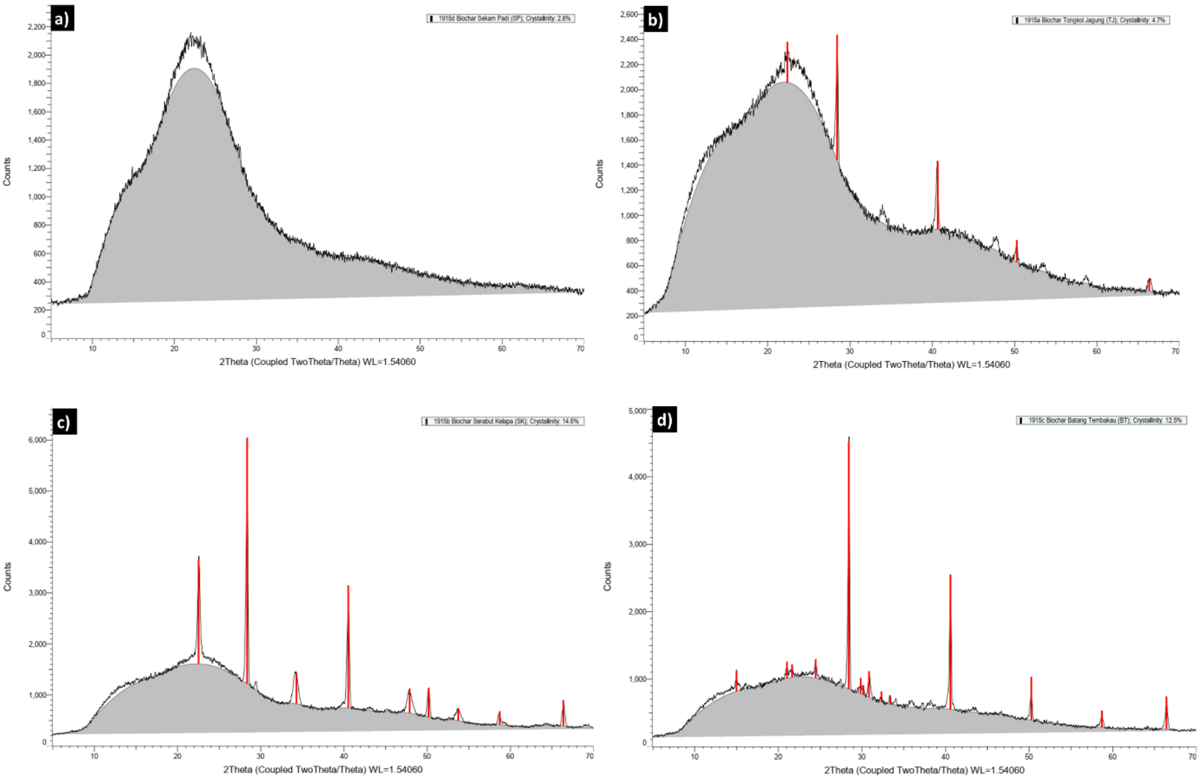

Figure 4. XRD graph for four types of biochar. a) RHB, b) CCB, c) CFB, d) TSB

CONCLUSION

This study finds that four types of biochar (rice husk, corn cob, coconut fibre, and tobacco stem) produced using a simple rotary kiln equipment have distinctive physicochemical characteristics. This was closely related to the pyrolysis conditions and the particular chemical composition of the feedstock. The interpretation of proximate analysis, chemical analysis, SEM, BET, FTIR, and XRD confirms that all biochars are dominated by amorphous structures with varying degrees of crystallinity and functional groups. Based on the assigned pyrolysis condition, rice husk biochar is more suitable for metal adsorption and as a silica soil amendment, while corn cob has high potential as an adsorbent for organic molecules. Moreover, coconut fibre and tobacco stem biochar have great potential for both CEC enhancement and carbon sequestration in soil due to their high resistance to microbial decomposition and their greater abundance of oxygen-containing functional groups. Many studies have found that corn cob can also improve soil CEC. It is recommended that further studies focus on optimising pyrolysis temperature and residence time using such simple equipment, and also evaluating the effectiveness of the biochar, especially in soil quality improvement in tropical semi-arid environments.

ACKNOWLEDGEMENTS

The authors declare no conflicts of interest related to work done in this study. The authors also wish to acknowledge the Institute of Research and Community Service (LPPM) University of Mataram for funding this research under the grant number 2487/UN18.L1/PP/2025.

REFERENCES

Adhikari, S., Moon, E., & Timms, W. (2024). Identifying biochar production variables to maximise exchangeable cations and increase nutrient availability in soils. *Journal of Cleaner Production*, *446*, 141454.

Ahmad, M., Lee, S. S., Dou, X., Mohan, D., Sung, J., Yang, J. E., & Ok, Y. S. (2012). Effects of pyrolysis temperature on soybean stover- and peanut shell-derived biochar properties and TCE adsorption in water. *BIORESOURCE TECHNOLOGY*, *118*, 536–544.

Ali, L., Manzoor, N., Li, X., Naveed, M., Nadeem, S. M., Waqas, R. M., Khalid, M., Abbas, A., Ahmed, T., Li, B., & Yan, J. (2021). Impact of Corn Cob-Derived Biochar in Altering Soil Quality, Biochemical Status and Improving Maize Growth under Drought Stress. *Agronomy*, *11*, 2300.

Almutairi, A. A., Ahmad, M., Rafique, M. I., & Al-wabel, M. I. (2023). Variations in composition and stability of biochars derived from different feedstock types at varying pyrolysis temperature. *Journal of the Saudi Society of Agricultural Sciences*, *22*(1), 25–34.

Anyebe, O., Sadiq, F. K., Manono, B. O., & Matsika, T. A. (2025). Biochar Characteristics and Application : Effects on Soil Ecosystem Services and Nutrient Dynamics for Enhanced Crop Yields. *Nitrogen*, *6*(2), 31.

Baldock, J. A., & Smernik, R. J. (2002). Chemical composition and bioavailability of thermally altered Pinus resinosa (Red pine) wood. *Organic Geochemistry*, *33*(9), 1093–1109.

Bu, X. L., Su, J., Xue, J. H., Wu, Y. B., Zhao, C. X., & Wang, L. M. (2019). Effect of rice husk biochar addition on nutrient leaching and microbial properties of Calcaric Cambisols. *Journal of Soil and Water Conservation*, *74*(2), 172–179.

Budai, A., Rasse, D. P., Lagomarsino, A., Lerch, T. Z., & Paruch, L. (2016). Biochar persistence, priming and microbial responses to pyrolysis temperature series. *Biology and Fertility of Soils*, *52*, 749–761.

Burachevskaya, M., Minkina, T., Bauer, T., Lobzenko, I., Fedorenko, A., Mazarji, M., Sushkova, S., Mandzhieva, S., Nazarenko, A., Butova, V., Wong, M. H., & Rajput, V. D. (2023). Fabrication of biochar derived from different types of feedstocks as an efficient adsorbent for soil heavy metal removal. *Scientific Reports*, *13:2020*.

Chatterjee, R., Sajjadi, B., Chen, W.-Y., Mattern, D. L., Hammer, N., Raman, V., & Dorris, A. (2020). Effect of Pyrolysis Temperature on PhysicoChemical Properties and Acoustic-Based Amination of Biochar for Efficient CO2 Adsorption. *Frontiers in Energy Research*, *8*.

Chen, B., Zeng, H., Yang, F., Yang, Y., Qiao, Z., Zhao, X., Wang, L., & Wu, F. (2024). Functional biochar as sustainable precursors to boost the anaerobic digestion of waste activated sludge from a circular economy perspective : a review. *Biochar*, *6:60*.

Claoston, N., Samsuri, A., Husni, M. A., & Amran, M. M. (2014). Effect of pyrolysis temperature on the physicochemical properties of empty fruit bunch and rice husk biochars. *Waste Management & Research*, *32*(4), 331–339.

Dai, Q., Li, J., Cao, Y., Wei, X., Tang, H., & Sun, J. (2020). Pyrolysis of Coconut Cloth in a Microwave Reactor : Effect of Pyrolysis Parameters on Product Yield and Characterization of Liquid Product and Biochar. *Bioresources*, *15*, 3737–3755.

de Carvalho Junior, J. I., Gonzaga, M. I. S., de Almeida, A. Q., Araújo, J., & Santos, L. C. O. (2019). Type and quantity of biochar influenced soil microbial activity and carbon priming effect. *Semina: Ciências Agrárias*, *40*(4), 1405–1416.

Dhar, S. A., Sakib, T. U., & Hilary, L. N. (2020). Effects of pyrolysis temperature on production and physicochemical characterization of biochar derived from coconut fiber biomass through slow pyrolysis process. *Biomass Conversion and Biorefinery*, *12*, 2631–2647.

Ernest, B., Yanda, P. Z., Hansson, A., & Fridahl, M. (2024). Long-term effects of adding biochar to soils on organic matter content, persistent carbon storage, and moisture content in Karagwe, Tanzania. *Scientific Reports*, *14*, 30565.

Fitri, H., Gürdil, G. A. K., Demirel, B., & Cevher, E. Y. (2023). Biomass potential from agricultural residues for energy utilization in West Nusa Tenggara (WNT), Indonesia. *GCB Bioenergy*, *15*(11), 1405–1414.

Flores-izquierdo, M. A., Carrera, O., Gaviria-restrepo, J., & Flores-Espinoza, B. C. (2025). Thermochemical conversion of avocado agro-industrial waste: Influence of operating conditions on biochar yield and properties. *Bioresource Technology Reports*, *32*, 102418.

Ghorbani, M., Amirahmadi, E., Neugschwandtner, R. W., Konvalina, P., Kopecký, M., Moudrý, J., Perná, K., & Murindangabo, Y. T. (2022). The Impact of Pyrolysis Temperature on Biochar Properties and Its Effects on Soil Hydrological Properties. *Sustainability*, *14*, 14722.

Glaser, B., Haumaier, L., Guggenberger, G., & Zech, W. (2001). The 'Terra Preta' phenomenon: a model for sustainable agriculture in the humid tropics. *Naturwissenschaften*, *88*, 37–41.

Gotore, O., Rameshprabu, R., & Itayama, T. (2022). Adsorption performances of corn cob-derived biochar in saturated and semi-saturated vertical- flow constructed wetlands for nutrient removal under erratic oxygen supply. *Environmental Chemistry and Ecotoxicology*, *4*, 155–163.

Goularte, M. D. P., Sousa, Á. F. De, Cholant, C., Romano, L., Labidi, J., Missio, A. L., Acosta, A., & Gatto, D. A. (2025). Pyrolysis of Rice Husk for the Production of Bioactive Compounds with Potential in Green Chemistry and Sustainable Agriculture. *Molecules*, *30*(13), 2754.

Gross, A., Bromm, T., Polifka, S., Fischer, D., & Glaser, B. (2024). Long-term biochar and soil organic carbon stability – Evidence from field experiments in Germany. *Science of the Total Environment*, *954*, 176340.

Guarnieri, S. F., do Nascimento, E. C., Junior, R. F. C., de Faria, J. L. B., & Lobo, F. de A. (2021). Coconut fiber biochar alters physical and chemical properties in sandy soils. *Acta Scientiarum: Agronomy*, *43*, e51801.

Hamidu, I., Afotey, B., Kwakye-awuah, B., & Adjah, D. (2025). Synthesis of silica and silicon from rice husk feedstock : A review. *Heliyon*, *11*(4), e42491.

Handiso, B., Paakkonen, T., & Wilson, B. P. (2024). Effect of pyrolysis temperature on the physical and chemical characteristics of pine wood biochar. *Waste Management Bulletin*, *2*, 281–287.

Ighalo, J. O., Ohoro, C. R., Ojukwu, V. E., Oniye, M., Shaikh, W. A., Biswas, J. K., Seth, C. S., Mohan, G. B. M., Chandran, S. A., & Rangabhashiyam, S. (2025). Biochar for ameliorating soil fertility and microbial diversity : From production to action of the black gold. *ISCIENCE*, *28*(1), 111524.

Irewale, A. T., Elemike, E. E., Shaik, A. M., Dimkpa, C. O., & Oguzie, E. E. (2025). Theoretical and experimental insights into BET surface area and pore analysis of water hyacinth biochar: Prospects for efficient bio - nanofertilizer development. *MRS Advances*, *10*, 1029–1035.

Jia, Y., Shi, S., Liu, J., Su, S., Liang, Q., Zeng, X., & Li, T. (2018). Study of the Effect of Pyrolysis Temperature on the Cd 2 + Adsorption Characteristics of Biochar. *Applied Sciences*, *8*(7), 1019.

Kabir, E., Kim, K.-H., & Kwon, E. E. (2023). Biochar as a tool for the improvement of soil and environment. *Frontiers in Environmental Science*, *11*, 1324533.

Kabore, A. B., Njoroge, W. K., Masika, E., Minjauw, M. M., Dendooven, J., Detavernier, C., & Adriaens, M. (2026). Comparative analysis of structural, physicochemical, and electrochemical properties of graphene oxide derived from commercial graphite and rice husk biomass for sensing applications. *Results in Materials*, *29*, 100867.

Kerner, P., Struhs, E., Mirkouei, A., Aho, K., Lohse, K. A., Dungan, R. S., & You, Y. (2023). Microbial Responses to Biochar Soil Amendment and Influential Factors: A Three-Level Meta-Analysis. *Environmental Science & Technology*, *57*(48), 19838–19848.

Khan, S., Irshad, S., Mehmood, K., Hasnain, Z., Nawaz, M., Rais, A., Gul, S., Wahid, M. A., Hashem, A., Abd_Allah, E. F., & Ibrar, D. (2024). Biochar Production and Characteristics, Its Impacts on Soil Health, Crop Production, and Yield Enhancement: A Review. *Plants*, *13*(2), 166.

Kim, S. S., Ly, H. V., Choi, G. H., Kim, J., & Woo, H. C. (2012). Pyrolysis characteristics and kinetics of the alga Saccharina japonica. *Bioresource Technology*, *123*, 445–451.

Kome, G. K., Enang, R. K., Yerima, B. P. K., & Lontsi, M. G. R. (2018). Geoderma Regional relating soil pH measurements in H2O, KCl and CaCl2 for volcanic ash soils of Cameroon. *Geoderma Regional*, *14*, e00185.

Kusnarta, I. G. M., Suwardji, S., Fahrudin, F., Sukartono, S., Wangiyana, W., Huda, B. N., Ismaranti, Y. M., Ismawati, Y. Y., Maharani, A., Fokke, B., & Bensaïah, C. (2024). Effectiveness of Different Sources of Biochar for Immobilizing Mercury in Soil from Artisanal and Small-Scale Gold Mining Areas in Taliwang Village of West Sumbawa Regency, Indonesia. *International Journal of Design & Nature and Ecodynamics*, *19*(5), 1627–1634.

Lago, B. C., Silva, C. A., Melo, L. C. A., & Morais, E. G. de. (2021). Predicting biochar cation exchange capacity using Fourier transform infrared spectroscopy combined with partial least square regression. *Science of The Total Environment*, *794*, 148762.

Li, Y., Liu, T., He, X., Liu, R., Xu, T., Hu, M., Gu, K., Su, J., & Zou, C. (2021). Tobacco Stalk Biochar Application Improves Soil Fertility and Flue- Cured Tobacco Growth. *Journal of Agroculture & Biology*, *25*, 632–638.

Martín-Lara, M. A., Munoz-Batista, M. J., Blazquez, G., Pereira, L., Quintana, A., & Calero, M. (2026). Turning plastic and biomass waste into adsorbents: CO2/CH4 separation and comparison with commercial carbons. *Waste Management*, *210*, 115223.

Meena, O. P., Patel, V. B., Singh, S. K., Singh, K., Mhetre, V. B., Dhar, S., Meena, M. C., Sanghwan, S., Rudra, S. G., Asrey, R., Vinod, B. R., & Saha, S. (2025). Harnessing agricultural waste and microbial synergy to improve soil function and fruit quality in 'Amrapali' mango. *Energy Nexus*, *20*, 100547.

Mobarak, M. Bin, Pinky, N. S., Mustafi, S., Chowdhury, F., Nahar, A., Akhtar, U. S., Quddus, M. S., Yasmin, S., & Alam, M. A. (2024). Unveiling the reactor effect: a comprehensive characterization of biochar derived from rubber seed shell via pyrolysis and in-house reactor. *RSC Advances*, *14*(41), 29848–29859.

Munzeiwa, W. A., Tsekoa, P., Kammies, L. R. D., Chelechele, K., Oluwalana-Sanusi, A. E., & Chaukura, N.

(2025). Influence of biomass baseline potential on biochar properties and performance for targeted applications. *Discover Water*, *5:77*.

Najafi-ghiri, M., Boostani, H. R., & Bijanzadeh, E. (2025). Influence of biochars and silica on K fractionations and release into CaCl 2, HCl and oxalic acid in a calcareous soil. *Scientific Reports*, *15*, 23329.

Nicholas, H. L., Mabbett, I., Apsey, H., & Robertson, I. (2025). Physico-chemical properties of waste derived biochar from community scale faecal sludge treatment plants Gates Open Research. *Gates Open Research*, *6:96*.

Peng, Y., Tian, Y., Li, Q., Li, S., Shi, X., Wang, K., & Fu, L. (2025). Influence of Expansion Pretreatment on the Structure Evolution and Reaction Chemistry during Oxidative Pyrolysis of Tobacco Biomass. *ACS Omoega*, *10*(18), 18552–18560.

Permadi, D. A., & Oanh, N. T. K. (2013). Assessment of biomass open burning emissions in Indonesia and potential climate forcing impact. *Atmospheric Environment*, *78*, 250–258.

Prasiefa, M. G., & Firmansyah, D. (2025). Physiochemical Performance and Structural Characterization of Tobacco Stem Biochar under Various Pyrolysis Conditions for Sustainable Fertilizer Development. *Indonesian Journal of Chemical Science*, *14*(3), 97–

Qin, Z., Luo, X., Rong, N., Wang, M., Wang, J., Wu, J., Li, Z., Duns, G. J., He, F., Chen, H., & Yang, L. (2016). Preparation and Analysis of Physicochemical Properties of Tobacco Stem Biochar. *Journal of Nanoscience and Nanotechnology*, *16*(12), 12237–12243.

Raza, M., Inayat, A., Ahmed, A., Jamil, F., Ghenai, C., Naqvi, S. R., Shanableh, A., Ayoub, M., Waris, A., & Park, Y.-K. (2021). Progress of the pyrolyzer reactors and advanced technologies for biomass pyrolysis processing. *Sustainability*, *13*(19), 11061.

Reddy, A. S., Kasa, V. P., Samal, B., Dubey, B. K., Yadav, V., & Pandey, D. S. (2025). Sustainable agricultural waste management in India: Innovations, challenges, and future perspectives. *Biomass and Bioenergy*, *202*, 108261.

Severo, F. F., da Silva, L. S., Moscôso, J. S. C., Sarfaraz, Q., Júnior, L. F. R., Lopes, A. F., Marzari, L. B., & Molin, G. D. (2020). Chemical and physical characterization of rice husk biochar and ashes and their iron adsorption capacity. *SN Applied Sciences*, *2*, 1286.

Sriphirom, P., Towprayoon, S., Yagi, K., Rossopa, B., & Chidthaisong, A. (2022). Changes in methane production and oxidation in rice paddy soils induced by biochar addition. *Applied Soil Ecology*, *179*, 104585.

Sukartono, Utomo, W. H., Nugroho, W. H., & Kusuma, Z. (2011). Simple Biochar Production Generated From Cattle Dung and Coconut Shell. *Journal of Basic and Applied Scientific Research*, *1*(10), 1680–1685.

Tag, A. T., Duman, G., Ucar, S., & Yanik, J. (2016). Effects of Feedstock Type and Pyrolysis Temperature on Potential Applications of Biochar. *Journal of Analytical and Applied Pyrolysis*, *120*, 200–206.

Tomczyk, A., Sokolowska, Z., & Boguta, P. (2020). Biochar physicochemical properties : pyrolysis temperature and feedstock kind effects. *Reviews in Environmental Science and Bio/Technology*, *19*(1), 191–215.

Tu, P., Zhang, G., Wei, G., Li, J., Li, Y., Deng, L., & Yuan, H. (2022). Influence of pyrolysis temperature on the physicochemical properties of biochars obtained from herbaceous and woody plants. *Bioresources and Bioprocessing*, *9:131*.

Vasilievici, G., Sanda, M., Băjan, M., Dusescu-Vasile, C., Onutu, I., Brănoiu, G., Bombos, D., Baioun, A., Borcea, A. F., & Stănică, A.-I. (2025). Synthesis and Characterization of Biochar Obtained by Partial Delignification of Waste Biomass. *Molecules*, *30*(23), 4505.

Wood, R., Masek, O., & Erastova, V. (2024). Developing a molecular-level understanding of biochar materials using public characterization data. *Cell Reports Physical Science*, *5*(7), 102036.

Xu, D., Luo, H., He, T., Yang, E., & Gao, J. (2025). Effects of long-term biochar application combined with chemical fertilization on the nitrifier community in tobacco plantation soil. *Frontiers in Microbiology*, *16*, 1720769.

Yang, C., Liu, J., & Lu, S. (2021). Pyrolysis temperature affects pore characteristics of rice straw and canola stalk biochars and biochar-amended soils. *Geoderma*, *397*, 115097.

Yıldız, Z., & Ceylan, S. (2018). Pyrolysis of tobacco factory waste biomass. *Journal of Thermal Analysis and Calorimetry*, *136*, 783–794.

Yuniwati, E. D., & Lestari, A. M. (2021). The treatment combination of corn cob biochar and bio land organic fertilizer as soil amendment in kale plant (Brassica oleraceae var. acephala L.). *AMCA Journal of Science and Technology*, *2*(1), 25–30.

Zhang, L., Tu, L., Liang, Y., Chen, Q., Li, Z., Li, C., Wang, Z., & Li, W. (2018). Coconut-based activated carbon fibers for efficient adsorption of various organic dyes. *RSC Advances*, *8*, 42280–42291.

Zhang, Y., Ye, C., Su, Y., Peng, W., Lu, R., Liu, Y., Huang, H., He, X., Yang, M., & Zhu, S. (2022). Soil Acidification caused by excessive application of nitrogen fertilizer aggravates soil-borne diseases: Evidence from literature review and field trials. *Agriculture, Ecosystems & Environment*, *340*, 108176.

Zhao, B., O'Connor, D., Zhang, J., Peng, T., Shen, Z., Tsang, D. C. W., & Hou, D. (2018). Effect of pyrolysis temperature, heating rate, and residence time on rapeseed stem derived biochar. *Journal of Cleaner*

Production, *174*, 977–987.
Zhao, L., Guan, H., Wang, R., Wang, H., Li, Z., Li, W., Xiang, P., & Xu, W. (2021). Effects of Tobacco Stem-Derived Biochar on Soil Properties and Bacterial Community Structure under Continuous Cropping of Bletilla striata. *Journal of Soil Science and Plant Nutrition*, *21*, 1318–1328.
Zhylina, M., Miroshnichenko, D., Melnykov, A., Stepanova, V., Lazdovica, K., Zemcenkovs, V., Sterna, V., & Ozolins, J. (2025). Biochar structure development during slow pyrolysis of pellets from barley straw and bran. *Scientific Reports*, *15*, 42624.